








Temperature-dependent photoluminescence dynamics of CsPbBr₃ and CsPb(Cl,Br)₃ perovskite nanocrystals in a glass matrix

E. V. Kulebyakina ¹, M. L. Skorikov ¹, E. V. Kolobkova ^{2,3}, M. S. Kuznetsova ⁴, M. N. Bataev ⁴,
D. R. Yakovlev ^{1,5,6} and V. V. Belykh ^{5,*}

¹*P.N. Lebedev Physical Institute of the Russian Academy of Sciences, 119991 Moscow, Russia*

²*St. Petersburg State Institute of Technology (Technical University), 190013 St. Petersburg, Russia*

³*ITMO University, 199034 St. Petersburg, Russia*

⁴*Spin Optics Laboratory, St. Petersburg State University, 198504 St. Petersburg, Russia*

⁵*Experimentelle Physik 2, Technische Universität Dortmund, 44221 Dortmund, Germany*

⁶*Ioffe Institute, Russian Academy of Sciences, 194021 St. Petersburg, Russia*



(Received 16 January 2024; revised 7 May 2024; accepted 14 May 2024; published 12 June 2024)

Lead halide perovskite nanocrystals (NCs) in a glass matrix combine excellent optical properties and stability against environment. The spectral and temporal characteristics of photoluminescence from CsPbBr₃ and CsPb(Cl,Br)₃ nanocrystals in a fluorophosphate glass matrix are measured in a temperature range from 6 to 270 K in order to reveal factors that determine their quantum yield and recombination dynamics. At low temperatures, the recombination dynamics is characterized by three decay components with timescales on the order of 1 ns, 10 ns, and 1 μs. The relative contributions of the corresponding processes and their characteristic times are strongly temperature dependent. The emission intensity decreases with growing temperature. This effect is stronger in smaller NCs, which highlights the role of surface states. These experimental results are discussed on the basis of a model taking into account the NC energy structure and the presence of electron and hole surface trap states. The photoluminescence dynamics at low temperatures is dominated by charge-carrier radiative recombination and relaxation to shallow traps. At temperatures exceeding 100 K, the dynamics is affected by carrier activation to the excited states.

DOI: [10.1103/PhysRevB.109.235301](https://doi.org/10.1103/PhysRevB.109.235301)

I. INTRODUCTION

Lead halide perovskite semiconductors are known for more than a century [1,2]. However, only recently they emerged as a promising platform for photovoltaic applications [3], which stimulated research in different directions revealing many advantages of perovskites [4,5]. Among them are defect tolerance [6], high quantum yield [7], high efficiency of spin orientation by light [8–12], ease of synthesis, and the possibility to form nanocrystals (NCs). In particular, perovskite NCs can be very promising for light-emitting devices [13]. They have relatively narrow emission spectrum with central wavelength controlled by the anion composition and NC size. However, colloidal lead halide perovskite NCs have rather poor stability when exposed to air, humidity, elevated temperatures, or intense light [6]. A promising approach to solve this problem is to synthesize all-inorganic lead halide perovskite NCs embedded in glass [14–19]. Especially suitable is the fluorophosphate glass matrix [20], which offers high chemical resistance to harmful environmental conditions and the ability to introduce high concentrations of halides ensuring also high quantum yield of NCs.

For the further development of perovskite-based light-emitting devices it is crucial to get physical insight into

processes that limit the quantum yield and radiative recombination rate in perovskite NCs in a glass matrix and to clarify how these parameters depend on the NC size and composition. To this end, it is straightforward to study spectra and dynamics of photoluminescence (PL) from NCs as a function of temperature. The temperature-dependent properties of the continuous-wave (cw) PL spectra of CsPbBr₃ NCs in a glass matrix at $T = 40\text{--}240$ K were investigated in Ref. [18], where, in particular, the activationlike decrease in the PL intensity and the broadening of the PL line with temperature were observed.

In this paper, we present systematic studies of the PL spectra and recombination dynamics down to liquid-helium temperatures for CsPbBr₃ and CsPb(Cl,Br)₃ NCs of different sizes embedded into a fluorophosphate glass matrix. On the basis of a model involving surface traps, we discuss factors responsible for PL decrease with an increase in temperature and for the observed complex PL dynamics. We find that an increase in the NC size leads to the enhancement of their spectral homogeneity and makes the PL intensity less sensitive to temperature. At the same time, with the introduction of Cl, PL temperature quenching becomes more pronounced.

II. EXPERIMENTAL DETAILS

Samples of fluorophosphate glass with composition of 40P₂O₅–35BaO–5NaF–10AlF₃–10Ga₃O₃ (mol.%) doped

*vasilii.belykh@tu-dortmund.de

with NaCl (BaCl₂), Cs₂O, PbF₂, and BaBr₂ were synthesized using the melt-quench technique. Glass synthesis was performed in a closed glassy carbon crucible at a temperature of 1000 °C. About 50 g of the batch was melted in a crucible for 30 min, then the glass melt was cast on a glassy carbon plate and pressed to form a plate with a thickness of 2 mm. CsPbBr₃ or CsPb(Cl,Br)₃ perovskite NCs were precipitated by glass self-crystallization during melt quenching and additional heat treatment at 400 °C. The size of NCs in the samples varied from 8 to 16 nm depending on the annealing time. The composition of the sample with chlorine was evaluated using the x-ray diffraction method to be close to CsPb(Cl_{0.5}Br_{0.5})₃ [21]. Also, supporting information of Ref. [21] contains data on TEM measurements for nominally identical sample giving size distribution of NCs.

For *PL measurements*, the samples were placed in a helium vapor-flow cryostat to achieve temperatures from 5 to 270 K. The steady-state PL spectra were recorded with a resolution of 0.9 meV using a grating spectrometer equipped with a liquid-nitrogen-cooled charge-coupled-device (CCD) matrix detector. The sample was excited using a cw semiconductor laser with a wavelength of 405 nm and a power of 2–5 μW. The size of the laser spot on the sample was about 200 μm.

An incandescent tungsten ribbon lamp was used to measure the optical *transmission spectra*. The investigated sample was thinned to 43 μm. The spectra were recorded using the same grating spectrometer with a liquid-nitrogen-cooled CCD detector.

The *PL dynamics* was measured with a Hamamatsu C5680 streak camera coupled to a grating spectrograph. The spectral resolution was typically about 4 meV, and the time resolution was about 0.01 of the measurement time range. In these measurements, the sample was excited at a wavelength of 400 nm by the second harmonic of 2.5-ps pulses from a Mira-900D mode-locked Ti:sapphire laser with a pulse repetition rate of 76 MHz, which could be lowered by a factor of 16–8192 using a pulse picker for time-resolved measurements in time ranges up to 100 μs. The size of the laser spot on the sample was about 0.5 × 0.3 mm and the pulse energy was about 0.5 pJ (corresponding to an average power of about 2 μW for a pulse repetition rate of 4.75 MHz). We checked that we work in the linear regime, i.e., the shape of the PL dynamics is independent of the excitation power.

For the investigation of the *PL excitation spectra*, the samples were placed in a helium closed-cycle cryostat and cooled to a temperature of 12 K. The PL was recorded using a spectrometer equipped with a liquid-nitrogen-cooled CCD camera. Optical excitation was carried out using light from an incandescent lamp transmitted through a premonochromator and focused onto the sample in a spot with a size of 2 mm. The excitation power was about 0.4 μW. The experimental data were normalized to the power of the incident light at a given wavelength. The spectral resolution of the PL excitation spectra was determined by the full width at half-maximum (FWHM) of the light band transmitted through the premonochromator, which was about 7 meV (1.5 nm).

The absolute quantum yield was measured with an Absolute PL Quantum Yield Measurement System C9920-02G-03G (Hamamatsu) consisting of a photonic multichannel analyzer PMA-12 with an InGaAs sensor (200–950 nm range

with 2-nm resolution), an integrating sphere unit A10104-01, a monochromatic light source L9799-01 with a 150 W Xenon light source, and remote-controlled monochromator (250–950 nm range, bandwidth from 2 to 5 nm). To avoid reabsorption, the samples had optical densities between 0.1 and 0.5 at the exciton peak wavelength. This low values were achieved by using glass powder, which was placed in a quartz cuvette. The luminescence excitation wavelength corresponded to the maximum in the luminescence excitation spectrum, which was 405 nm.

III. PHOTOLUMINESCENCE UNDER CONTINUOUS-WAVE EXCITATION

We show the results for three samples with CsPbBr₃ NCs of different sizes and for one sample with CsPb(Cl,Br)₃ NCs. The summary of NC parameters is presented in Table I. The PL spectra at a temperature of 6 K for the samples under study are shown in Fig. 1(a). The energy of the PL maximum is controlled by the band gap of the material, the quantum confinement energy of electrons and holes in NCs, and the Coulomb interaction energy between electron and hole (exciton binding energy). In particular, for the set of samples with CsPbBr₃ NCs, different PL peak energies correspond to different NC sizes D . A decrease in the NC size from 16 to 9 nm for CsPbBr₃ NCs leads to a shift of the PL peak energy from 2.36 to 2.44 eV as a result of stronger quantum confinement. Meanwhile, the introduction of Cl further shifts the PL peak energy to 2.73 eV, as seen from the PL spectrum of CsPb(Cl,Br)₃ NCs with $D = 8$ nm. It is also apparent that the FWHM of the PL line increases with a decrease in the NC size. This is related to the fact that the low-temperature (below 50 K) PL linewidth is determined by inhomogeneous broadening arising from the spread in the NC sizes. For small values of D , the PL peak energy is more sensitive to the variation of D , which results in larger inhomogeneous broadening [see Eqs. (1) and (2) below]. The linewidth is varied from 12 meV for CsPbBr₃ NCs with $D = 16$ nm up to 55 meV for NCs with $D = 9$ nm.

The energy structure of NCs becomes more apparent from the PL excitation spectra. Figures 1(d)–1(f) show the PL intensity for the samples with different NC sizes as a function of the detection energy and excitation energy. The PL has a maximum when the detection energy corresponds to the NC ground state and the excitation energy corresponds to either ground or one of the excited states. For each state, the excitation energy corresponding to the PL maximum linearly increases with the detection energy as shown by dashed lines. This is related to the distribution over NC sizes within the ensemble. Different sizes along the PL distribution corresponding to the excitation into the first excited optically active state are marked in Fig. 1(d). For the sample with the largest average NC size and the smallest inhomogeneous broadening, up to five energy levels are resolved in the PL excitation spectrum [Fig. 1(g)]. These levels correspond to states with different orbital quantum numbers, and their energies are well reproduced by the model of a spherical quantum dot with infinite energy barriers presented in the Supplemental Material [22] (see also Refs. [23–25]). The half of the difference between the position of the first excited optically active state determined from the

TABLE I. Summary of the NC parameters. FWHM is the PL line full width at half-maximum at $T = 6$ K [equal to Γ_{inh} in Eqs. (2) and (3)], E_a is the linewidth activation energy, γ_{ph} is the strength of electron-phonon coupling, and τ_r is the exciton recombination time corresponding to the fast component in the PL dynamics at $T = 6$ K. The quantum yield is measured at room temperature.

No.	Composition	Size (nm)	PL peak energy (eV)	FWHM, Γ_{inh} (meV)	E_a (meV)	γ_{ph} (fs $^{-1}$)	τ_r (ns)	Quantum yield (%)
1	CsPb(Cl $_{0.5}$ Br $_{0.5}$) $_3$	8	2.73	32	28	0.07	0.33	5
2	CsPbBr $_3$	9	2.441	55	47	0.16	1.1	61
3	CsPbBr $_3$	12	2.391	41	29	0.06	0.95	78
4	CsPbBr $_3$	16	2.361	12	15	0.03	0.55	85

PL excitation spectrum and the exciton energy of 2.32 eV in bulk CsPbBr $_3$ [8,28] is used to determine the average NC size for a given sample. This method is insensitive to the Stokes shift that reduces the PL peak energy. However, we assume the same exciton binding energy for different NC sizes and quantum confined states, because its variation is small compared to the quantum confinement energy.

With an increase in temperature, the PL spectrum is transformed as shown in Fig. 1(b) for CsPb(Cl,Br) $_3$ NCs. The energy of the PL peak shifts and the line broadens. Note that the PL spectra in Fig. 1(b) are normalized to their maximal intensity at the given temperature, while the integrated intensity varies with temperature (see below). It is noteworthy that

the PL peak energy increases with temperature, in contrast to conventional semiconductors like GaAs. At high temperatures, above 200 K, this increase changes to a slight decrease. For CsPbBr $_3$ NCs, the corresponding spectra presented in the Supplemental Material [22] show similar behavior with temperature. The transmission spectrum of the CsPb(Cl,Br) $_3$ sample experiences similar evolution [Fig. 1(c)]: the transmission minimum, corresponding to the exciton resonance, shifts to higher energy and broadens with increasing temperature.

The temperature dependence of the integrated PL intensity for different samples is shown in Fig. 2(a). Interestingly, below 40 K the intensity increases with temperature. Then it stays approximately constant in the range of 40–140 K,

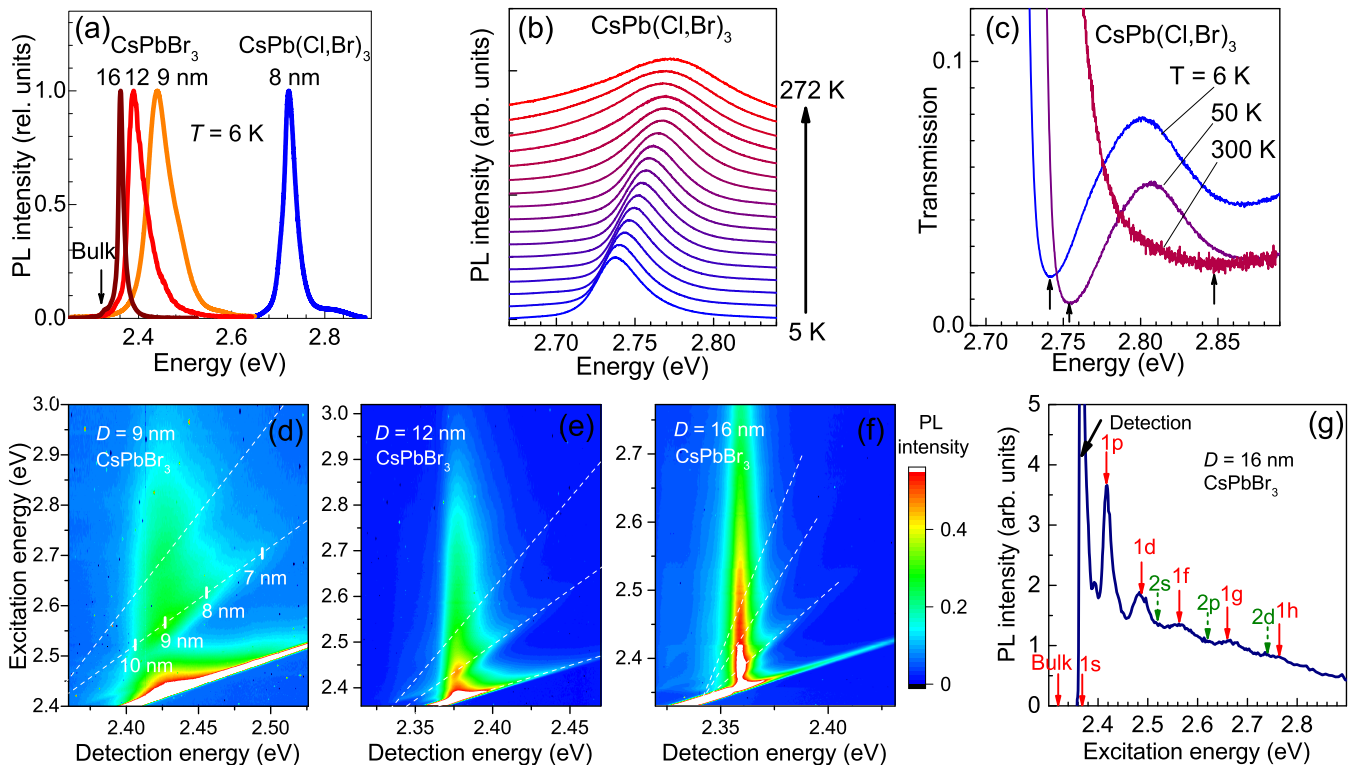


FIG. 1. (a) PL spectra of CsPbBr $_3$ and CsPb(Cl,Br) $_3$ NCs with different sizes in a fluorophosphate glass matrix at $T = 6$ K. Arrow shows the exciton energy in bulk CsPbBr $_3$, equal to 2.32 eV. (b) PL and (c) transmission spectra of CsPb(Cl,Br) $_3$ NCs at different temperatures. PL spectra are normalized to the respective peak values and shifted vertically for clarity. Arrows indicate transmission minima corresponding to the exciton resonance. (d)–(f) PL excitation spectrum maps for CsPbBr $_3$ NCs of different sizes showing the PL intensity as a function of the detection energy and excitation energy. Dashed lines are guides for the eye showing optical transitions corresponding to the excited states for NCs with different sizes present in the sample. Vertical markers in (d) show the calculated NC sizes for the corresponding excitation and detection energies. (g) PL excitation spectrum at the detection energy of 2.37 eV for CsPbBr $_3$ NCs with size of 16 nm. Arrows show the positions of bulk perovskite PL peak energy, the detection energy, and the energy levels calculated for spherical NCs (see Supplemental Material [22]).

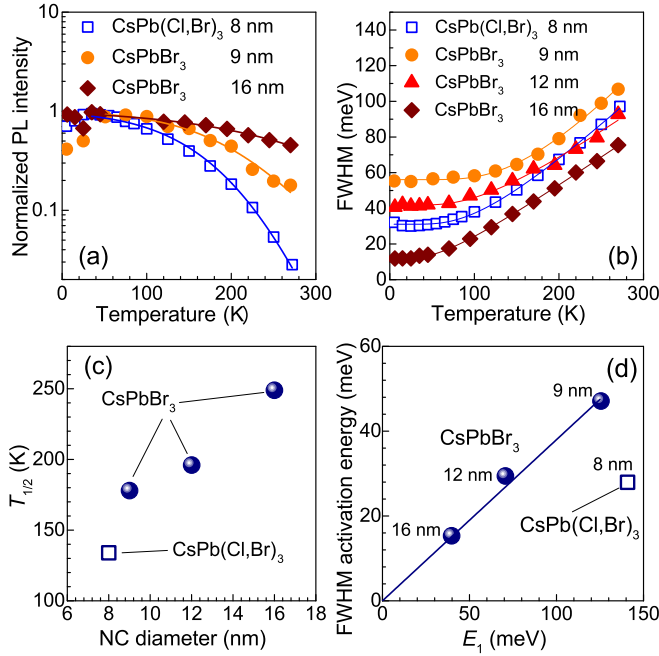


FIG. 2. Temperature dependencies of (a) integrated PL intensity and (b) FWHM of the PL peak for the studied samples. Solid lines show fits with Eq. S10 in the Supplemental Material [22] and Eq. (3) to the experimentally determined intensities and FWHM, respectively. (c) Dependence of the temperature at which intensity decreases twice from its maximal value on the NC diameter. (d) Activation energies E_a determined from the temperature dependencies of FWHM as a function of NC quantum confinement energy [see Eqs. (1) and (3)]. Line is a linear fit. Balls in (c) and (d) correspond to CsPbBr₃ NCs, while open square corresponds to CsPb(Cl,Br)₃ NCs.

and decreases at still higher temperatures. We attribute the intensity variation with temperature to carrier activation to deep-level surface centers where they can recombine nonradiatively [29–31]. This is discussed in detail in the following sections. We note that the rate of the high-temperature decrease in the PL intensity depends on the NC size and composition. We characterize this rate by the temperature $T_{1/2}$ at which the integrated PL intensity decreases to 50% of its maximal value. Figure 2(c) shows the dependence of $T_{1/2}$ on the NC diameter D . For the series of CsPbBr₃ samples, $T_{1/2}$ increases with D from 180 K for $D = 9$ nm to 250 K for $D = 16$ nm. The fact that nonradiative recombination is more pronounced in smaller NCs validates the assumption about the surface origin of nonradiative centers in these samples. One can also see that the high-temperature decrease in the PL intensity in CsPb(Cl,Br)₃ NCs is significantly faster than in CsPbBr₃ NCs of similar size. This may result from the increased density of nonradiative centers for NCs containing Cl.

The temperature dependence of the PL FWHM for different samples is shown in Fig. 2(b). The steady increase in the FWHM with T is related to lifetime shortening caused by carrier activation from the ground state to excited states via phonon absorption. The corresponding activation energies as a function of the quantum confinement energy in NCs are shown in Fig. 2(d).

IV. PHOTOLUMINESCENCE DYNAMICS

Next, we study the PL dynamics of the perovskite NCs under pulsed excitation. Figure 3 shows the spectrally integrated PL dynamics of CsPb(Cl,Br)₃ NCs at different temperatures in different time ranges. The dynamics is characterized by several components whose amplitudes and decay times depend on temperature. The fastest component with decay time of about 0.3 ns dominates at temperatures below 60 K, then disappears, and becomes important again above 150 K [Fig. 3(a)]. The next component is characterized by a decay time of about 10 ns at $T = 25$ K [Fig. 3(b)]. It is weak at low temperatures and dominates at higher temperatures. The decay time of the slowest component is as long as 10 μ s at low temperatures [Fig. 3(c)] and drastically shortens with an increase in temperature, while its relative amplitude increases. For each temperature, a multiexponential fit was carried out to determine the characteristic decay times. The decay times of the three components as a function of temperature are shown by symbols in Figs. 3(d) and 3(e) for CsPb(Cl,Br)₃ and CsPbBr₃ NCs, respectively. It is interesting that the decay time of the slowest component first drastically decreases and then slightly increases with temperature. Qualitatively similar multicompartment PL dynamics with similar temperature dependencies of the decay times is observed for other CsPbBr₃ NC samples.

V. DISCUSSION

Here we outline a systematic picture of the PL properties of perovskite NCs, i.e., of the broadening and thermal quenching of the PL lines and the PL dynamics. The most straightforward and expected observation is the increase in the PL peak energy and inhomogeneous broadening of the PL line with a decrease in the average size of NCs [Fig. 1(a)]. The dependence of the PL energy on the NC size D can be evaluated from the model of a spherically symmetric quantum dot with abrupt infinite potential barriers presented in the Supplemental Material [22]. According to this model, the ground-state energy of a NC is

$$E_1 = \frac{2\pi^2\hbar^2}{\mu D^2}, \quad (1)$$

where $1/\mu = 1/m_e + 1/m_h$ is the reduced mass, and we neglect the excitonic effect. The dependence of Eq. (1) was experimentally verified in Ref. [32] for centrifugated colloidal CsPbBr₃ NCs. Note that, in this model, the separation between the ground and the first excited optically active states is equal to the quantum confinement energy of the ground state E_1 , and this fact is used to determine the NC average size from the PL excitation spectrum. The validity of the model was verified by the fact that it allows also to calculate further NC excited states, giving good agreement with their measured positions in the excitation spectrum [Fig. 1(g)].

Then, the inhomogeneous broadening, which determines the PL linewidth Γ_{inh} at low temperatures and arises from the spread of the NC sizes ΔD , can be evaluated using Eq. (1) as $\Gamma_{\text{inh}} = |\partial E_1 / \partial D| \Delta D$:

$$\Gamma_{\text{inh}} = \frac{4\pi^2\hbar^2\Delta D}{\mu D^3}. \quad (2)$$

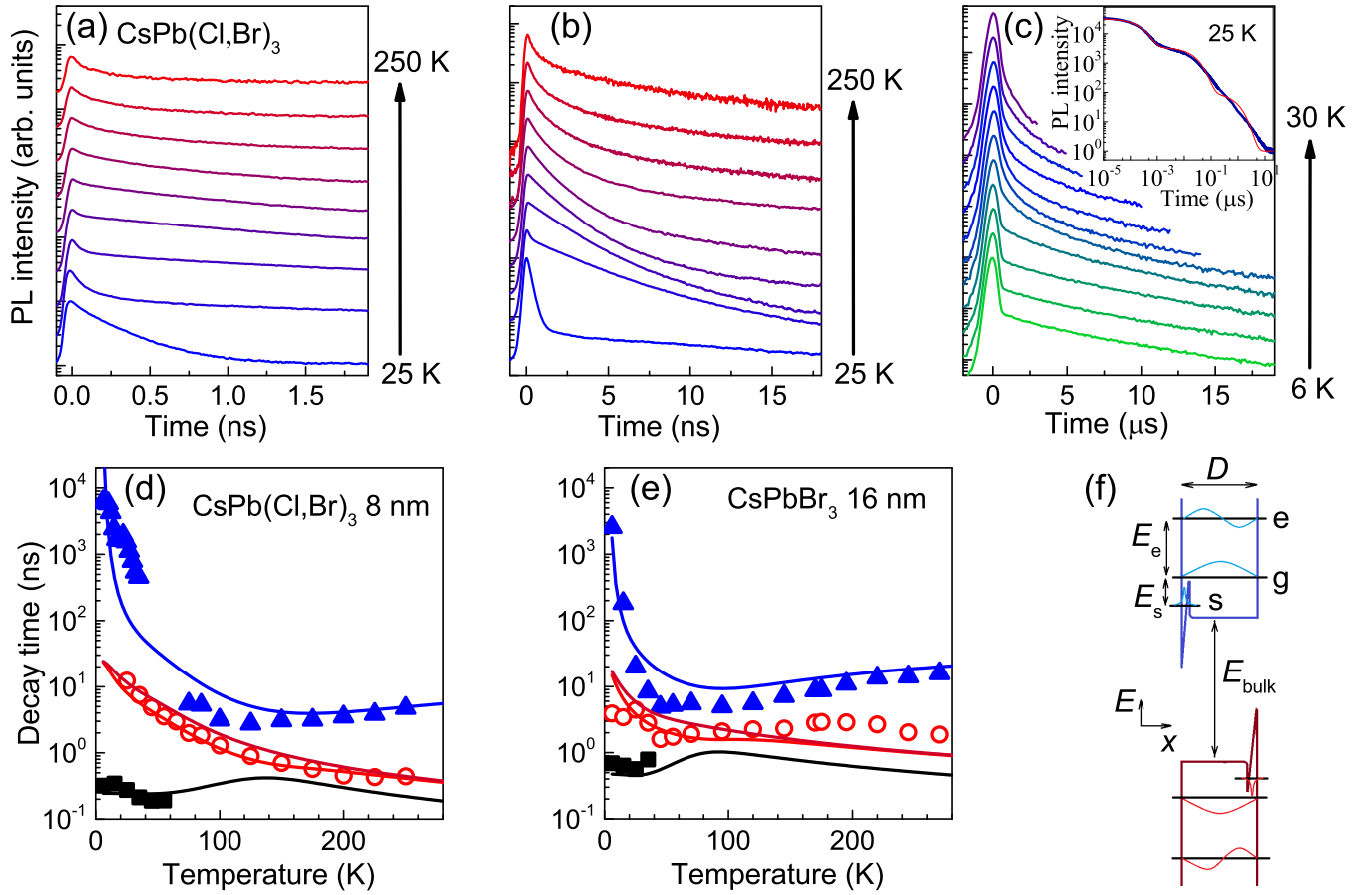


FIG. 3. (a)–(c) Spectrally integrated PL dynamics of $\text{CsPb}(\text{Cl},\text{Br})_3$ NCs at different temperatures in different time ranges. The curves are shifted vertically for clarity. Inset in (c) shows the dynamics at 25 K on the double-logarithmic scale together with the triple-exponential fit shown by red line. (d), (e) Temperature dependencies of the PL decay times for (d) 8-nm $\text{CsPb}(\text{Cl},\text{Br})_3$ NCs and (e) 16-nm CsPbBr_3 NCs. Symbols show experimental data, lines are the fits with the rate-equation model described in the Supplemental Material [22]. (f) Schematic band diagram and energy levels in NCs. A NC is represented as a spherical potential well with infinite walls (see Supplemental Material [22]). The diagram shows energy as a function of only one coordinate. Ground “g” and excited “e” states are shown both for the electron (top) and hole (bottom). Both electron and hole have potential trap near the surface with energy level “s” slightly below the ground state. Also the envelopes of the wave functions at these levels are shown.

So, the narrowest PL line is obviously obtained in the largest NCs [32], emitting at the lowest energies; for 16-nm CsPbBr_3 NCs, the FWHM is as small as 12 meV. Note that inhomogeneous broadening of the PL line in $\text{CsPb}(\text{Cl},\text{Br})_3$ NCs is twice smaller than that in CsPbBr_3 NCs of similar size.

The PL linewidth increases with temperature [Fig. 2(b)]. This is explained by the dephasing of the exciton ground state in the NCs caused by the phonon-assisted transitions of electrons and holes to higher energy levels. This behavior is commonly described by the relation

$$\Gamma(T) = \Gamma_{\text{inh}} + 2\gamma_{\text{ph}} \frac{1}{\exp(E_a/k_B T) - 1}. \quad (3)$$

Here, γ_{ph} characterizes the strength of electron-phonon coupling (factor 2 comes from the fact that Γ is FWHM), the energy E_a that determines the Bose-Einstein occupancy factor $[\exp(E_a/k_B T) - 1]^{-1}$ is the energy of the polar longitudinal-optical (LO) phonon mode, and we neglect the contribution from acoustical phonons. The values obtained from the fit are given in Table I. This relation is well established for systems

with continuous energy spectrum, where scattering by LO phonons simply limits the lifetime of radiative excitonic states (see, e.g., [33]). This relation also describes systems with discrete energy spectrum, such as epitaxial and colloidal quantum dots [34,35]. Although no real transitions can generally be induced by LO phonons in this case, dephasing caused by virtual transitions involving excited states (i.e., by the off-diagonal terms of the electron-phonon coupling Hamiltonian) leads to the behavior numerically well described by Eq. (3) [36].

The perovskite crystal lattice features a great number of optical phonon modes, and it is not *a priori* clear if this simple formula can be valid in this case. However, a number of studies indicate that only one of the optical-phonon modes of this lattice possesses a large dipole moment and, therefore, is dominant in the Fröhlich carrier-phonon interaction [37–39]. For CsPbBr_3 , the energy of this mode is about $E_{\text{LO}}^{\text{eff}} = 20$ meV [39]. Correspondingly, it was found that the temperature dependence of the PL linewidth in bulk and NC perovskite materials can be described by Eq. (3) with E_a on the same order of magnitude (e.g., [38,40]).

The PL linewidth in our samples [Fig. 2(b)] can also be well fitted with Eq. (3). The values obtained from the fit are given in Table I. However, one can see that the activation energy E_a is not simply a constant that can be associated with the energy of a specific phonon mode. Only for the largest CsPbBr₃ NCs E_a is close to E_{LO}^{eff} , while it is noticeably larger for smaller NCs. The dependence of E_a on the electron-hole pair quantum-confinement energy E_1 in the NCs [the latter is calculated by Eq. (1)] is shown in Fig. 2(d) and, for the series of CsPbBr₃ samples, follows a linear relation $E_a = 0.4E_1$. We note that, in a quantum dot with infinite potential barriers, the carrier ground-state energy with respect to the bottom of the potential is almost equal to the separation between the ground and first excited states (see the Supplemental Material [22]). Then, for an electron-hole pair, the energy of the first excited state (when either of carriers is on the next energy level, this state is not optically active) is equal to $1.5E_1$. Therefore, the value of E_a is close to the separation between the ground and first excited states of an electron-hole pair, which equals $0.5E_1$. The significance and, to that end, the universality of this relation [note that the point corresponding to the CsPb(Cl,Br)₃ sample deviates considerably] is the subject of further investigation. However, it may be speculated that this behavior occurs because there actually exist contributions from more than just one phonon mode to the dephasing rate, and the mode resonant with the energy of transitions from the ground to the first excited state has the greatest impact on $\Gamma(T)$. Hence, this transition energy enters Eq. (3).

The decrease in the PL intensity with increasing temperature [Fig. 2(a)] is a general feature that is observed in many semiconductor structures, including perovskite NCs [18,19,41–45] and single crystals [46]. It is often attributed to the activation of nonradiative recombination with temperature [18,42]. Usually the latter process is accompanied by a corresponding shortening of the PL decay time. This is not the case in our experiments. For example, for CsPb(Cl,Br)₃ NCs the PL intensity drops by more than an order of magnitude as the temperature is increased from 100 to 270 K [Fig. 2(a)]. Meanwhile, the short decay time decreases by only a factor of 3, and the long decay time even increases [Fig. 3(d)]. To understand the observed quenching we consider an inhomogeneous NC ensemble with a large spread in the rates of nonradiative recombination. The PL dynamics in “bright” NCs with the slowest nonradiative recombination will still be determined by radiative processes, while PL in “dark” NCs with the fastest nonradiative recombination will decay so rapidly that we cannot detect it. Under reasonable assumptions, discussed in the Supplemental Material [22], most of the NCs will fall into one of the two categories with the boundary between them shifting with temperature. Therefore, an increase in temperature will just lead to an increase in the number of NCs that recombine predominantly nonradiatively and do not contribute to PL and, thus, have no effect on the PL dynamics. This may take place in the following two scenarios which imply the existence of nonradiative states separated by relatively high potential barriers from band states. We remind that the fact that temperature quenching is more pronounced for smaller NCs suggests localization of nonradiative states near the surface. An example of such a state with a barrier resulting from adiabatic potentials in a defect is described in

Ref. [47]: the excited state of the defect is close to the NC ground state, while a carrier can be trapped to the deep defect ground state by overcoming a relatively high potential barrier as the temperature is increased. In the first scenario, the carrier captured by a surface trap recombines nonradiatively with the carrier remaining in the core. In the second scenario, the NCs contain resident carriers that are captured by the surface at higher temperatures (sufficient to overcome the potential barrier) and assist the Auger nonradiative recombination of photoexcited electron-hole pairs, which is very efficient for NCs with sharp confining potential [48]. Similar explanation was proposed for the temperature quenching of the quantum yield in CdSe/CdS colloidal NCs in Ref. [49], where the PL decay time showed an increase with temperature.

The reduction of the PL intensity with temperature is fitted with the model outlined above and elaborated in the Supplemental Material [22] [solid lines in Fig. 2(a)] assuming a Gaussian distribution of trap barrier energies. The fit shows good agreement with experimental data, better than simple Arrhenius-type equation [red dashed line in Fig. S1(b) of the Supplemental Material [22]] which is often used in the literature to fit temperature dependencies of the PL intensity [18,42]. The fact that the data for the three CsPbBr₃ NCs samples having different average NCs sizes is well fitted assuming the same surface density of the nonradiative centers confirms their surface origin. Furthermore, the QY of NCs increases with the NC size (Table I). We note that the room-temperature QY is larger than the efficiency expected from the reduction of the PL intensity with temperature [Fig. 2(a)]. This is explained by the fact that the QY is measured on powdered samples, while PL measurements were done on bulk samples and are affected by self-absorption.

To explain the multiscale PL dynamics of the NCs, we take into account the following considerations. In the low-temperature regime, the excited states do not contribute to the PL dynamics since they are separated by several tens of meV from the ground state. Nevertheless, even at low temperatures the dynamics is rather complicated, which cannot be explained by recombination from the ground state only. The presence of a long component with a lifetime strongly dependent on T [blue triangles at $T < 50$ K in Figs. 3(d) and 3(e)] suggests the existence of dark exciton states with suppressed radiative recombination (and therefore long-lived). A long-lived component demonstrating similar behavior with temperature was found for CsPbBr₃ and CsPbI₃ NCs and was attributed to the activation from a dark exciton state lying several meV below the bright state [50]. The dark state may be attributed to the spin-forbidden exciton state [50,51]. However, this cannot explain the existence of the intermediate component with a decay time of about 10 ns. A dark exciton state was indeed observed in the study of charge-carrier spin dynamics in the same CsPb(Cl,Br)₃ sample as presently investigated [52]. Based on an extremely small value of the electron-hole exchange splitting and the fact that the PL lifetime was independent of the magnetic field, this state was attributed in Ref. [52] to the spatially indirect exciton which forms when one of the carriers is captured by a shallow potential trap at the NC surface. These shallow states might result from excited states of the above-mentioned defect [47]. At low temperatures, carriers are unable to overcome

the potential barrier and to be trapped to the ground state of the deep defect. Thus, at low temperatures, the following electron-hole pair states should be included in the analysis: (i) both the electron and hole in the ground state of the NC, (ii) both in the respective shallow trap states, and (iii) either carrier is in the ground and the other in the trap state. The rate-equation model, considering phonon-induced transitions between these states, is presented in the Supplemental Material [22]. It yields reasonably good fits for the temperature dependencies of the experimentally observed decay times, shown by lines in Figs. 3(d) and 3(e). As far as the electron-hole wave-function overlap is small in the second and third cases, we assume that only state (i) is radiative, and the shortest, ~ 1 ns, PL component corresponds to the radiative recombination accompanied by relaxation from this state to state (iii). The PL decay rate at this stage approximately equals the radiative recombination rate γ_r . The intermediate, ~ 10 ns, PL component corresponds to the relaxation of either carrier from the NC ground to the surface trap state with the rate γ_{sg} , while the second carrier is already in the trap. Similar rate of carrier trapping was reported in Ref. [29] for $\text{CH}_3\text{NH}_3\text{PbBr}_3$ NCs. We note that the model predicts PL components with very close decay times in the intermediate range [red curves in Figs. 3(d) and 3(e)] which can hardly be separated in the experiment. It is important that the model fails to predict the intermediate component if traps for only one type of carriers are present. Finally, the long component corresponds to carrier activation from the trap to the NC ground state with time $\gamma_{sg}^{-1} \exp(E_s/k_B T)$ (which leads to recombination whenever both carriers happen to be activated), where E_s is the trap depth [Fig. 3(e)]. We also mention that the initial increase in the integrated PL intensity with T [Fig. 2(a)] may be related to the nonradiative recombination of carriers in these shallow traps. Indeed, at low temperatures carriers spend most of their time in trap states (having more chances to recombine nonradiatively) and are activated to the NC ground state at higher temperatures.

Another pronounced feature of the PL dynamics is the increase in the decay time at high temperatures (above 100 K). This is a common feature for systems with continuous density of states such as quantum wells [53,54]. There it is related to the filling with temperature of the reservoir of nonradiative exciton states with momenta beyond the light cone, while only excitons with momenta within the light cone and, thus, with low energy can recombine radiatively. We note that an

increase in the PL lifetime with temperature was also observed in nanocrystals [49]. Much like in other systems, we attribute this increase to the activation of carriers to excited states, where their recombination is inhibited. As the ground-state occupancy decreases with temperature, so does the recombination rate.

VI. CONCLUSIONS

To conclude, we have studied the optical properties of CsPbBr_3 and $\text{CsPb}(\text{Cl},\text{Br})_3$ NCs in a glass matrix: stationary PL and PL excitation spectra, transmission spectra, and PL dynamics. We have shown that an increase in the NC size results in weaker inhomogeneous broadening of the PL line corresponding to excitons. The exciton linewidth has activationlike dependence on temperature with an activation energy close to the interlevel separation in the NCs. We have observed PL quenching with temperature that is not accompanied by an increase in the PL decay rate. We show that this quenching is related to the existence of deep surface states acting as non-radiative recombination centers and separated by a potential barrier from band states. It becomes more pronounced with a decrease in the NC size and the introduction of Cl. For the largest CsPbBr_3 NCs, the PL intensity decreases by only 50% upon an increase in temperature from 6 to 270 K, which gives evidence of their high quality. The fact that thermal quenching of PL is enhanced for smaller NCs indicates that the number of nonradiative recombination centers in the bulk is small and they are mostly located at the surface. The PL dynamics of the studied NCs at low temperatures (below 50 K) is characterized by three timescales on the order of 1 ns, 10 ns, and 1 μs , respectively. This dynamics is described by a model considering relaxation of both electrons and holes to shallow traps and their thermal activation from the ground to the excited states.

ACKNOWLEDGMENTS

We are grateful to I. V. Ignatiev for careful reading of the manuscript and for useful remarks. We acknowledge financial support by the Ministry of Science and Higher Education of the Russian Federation, Contract No. 075-15-2021-598 at the P.N. Lebedev Physical Institute. The work of M.S.K. (sample characterization) was supported by the Saint Petersburg State University through Research Grant No. 122040800257-5.

-
- [1] H. L. Wells, Über die Cäsium und Kalium Bleihalogenide, *Z. Anorg. Chem.* **3**, 195 (1893).
 - [2] C. K. Moller, Crystal structure and photoconductivity of Cæsium plumbobalides, *Nature (London)* **182**, 1436 (1958).
 - [3] M. A. Green, A. Ho-Baillie, and H. J. Snaith, The emergence of perovskite solar cells, *Nat. Photonics* **8**, 506 (2014).
 - [4] *Halide Perovskites for Photonics: Recent History and Perspectives*, edited by A. Vinattieri and G. Giorgi (AIP Publishing, Melville, New York, 2021).
 - [5] *Hybrid Organic Inorganic Perovskites: Physical Properties and Applications*, edited by Z. V. Vardeny and M. C. Beard (World Scientific, Singapore, 2022).
 - [6] H. Huang, M. I. Bodnarchuk, S. V. Kershaw, M. V. Kovalenko, and A. L. Rogach, Lead halide perovskite nanocrystals in the research spotlight: stability and defect tolerance, *ACS Energy Lett.* **2**, 2071 (2017).
 - [7] C. M. Sutter-Fella, Y. Li, M. Amani, J. W. Ager, F. M. Toma, E. Yablonovitch, I. D. Sharp, and A. Javey, High photoluminescence quantum yield in band gap tunable bromide containing mixed halide perovskites, *Nano Lett.* **16**, 800 (2016).
 - [8] V. V. Belykh, D. R. Yakovlev, M. M. Glazov, P. S. Grigoryev, M. Hussain, J. Rautert, D. N. Dirin, M. V. Kovalenko, and M. Bayer, Coherent spin dynamics of electrons and holes in CsPbBr_3 perovskite crystals, *Nat. Commun.* **10**, 673 (2019).

- [9] P. Odenthal, W. Talmadge, N. Gundlach, R. Wang, C. Zhang, D. Sun, Z.-G. Yu, Z. Vally Vardeny, and Y. S. Li, Spin-polarized exciton quantum beating in hybrid organic inorganic perovskites, *Nat. Phys.* **13**, 894 (2017).
- [10] P. S. Grigoryev, V. V. Belykh, D. R. Yakovlev, E. Lhuillier, and M. Bayer, Coherent spin dynamics of electrons and holes in CsPbBr₃ colloidal nanocrystals, *Nano Lett.* **21**, 8481 (2021).
- [11] E. Kirstein, D. R. Yakovlev, M. M. Glazov, E. Evers, E. A. Zhukov, V. V. Belykh, N. E. Kopteva, D. Kudlacik, O. Nazarenko, D. N. Dirin, M. V. Kovalenko, and M. Bayer, Lead dominated hyperfine interaction impacting the carrier spin dynamics in halide perovskites, *Adv. Mater.* **34**, 2105263 (2022).
- [12] E. Kirstein, N. E. Kopteva, D. R. Yakovlev, E. A. Zhukov, E. V. Kolobkova, M. S. Kuznetsova, V. V. Belykh, I. A. Yugova, M. M. Glazov, M. Bayer, and A. Greilich, Mode locking of hole spin coherences in CsPb(Cl,Br)₃ perovskite nanocrystals, *Nat. Commun.* **14**, 699 (2023).
- [13] L. Protesescu, S. Yakunin, M. I. Bodnarchuk, F. Krieg, R. Caputo, C. H. Hendon, R. X. Yang, A. Walsh, and M. V. Kovalenko, Nanocrystals of cesium lead halide perovskites (CsPbX₃, X = Cl, Br, and I): novel optoelectronic materials showing bright emission with wide color gamut, *Nano Lett.* **15**, 3692 (2015).
- [14] S. Liu, Y. Luo, M. He, X. Liang, and W. Xiang, Novel CsPbI₃ QDs glass with chemical stability and optical properties, *J. Eur. Ceram. Soc.* **38**, 1998 (2018).
- [15] S. Liu, M. He, X. Di, P. Li, W. Xiang, and X. Liang, Precipitation and tunable emission of cesium lead halide perovskites (CsPbX₃, X = Br, I) QDs in borosilicate glass, *Ceram. Int.* **44**, 4496 (2018).
- [16] P. Li, C. Hu, L. Zhou, J. Jiang, Y. Cheng, M. He, X. Liang, and W. Xiang, Novel synthesis and optical characterization of CsPb₂Br₅ quantum dots in borosilicate glasses, *Mater. Lett.* **209**, 483 (2017).
- [17] B. Ai, C. Liu, J. Wang, J. Xie, J. Han, and X. Zhao, Precipitation and optical properties of CsPbBr₃ quantum dots in phosphate glasses, *J. Am. Ceram. Soc.* **99**, 2875 (2016).
- [18] B. Ai, C. Liu, Z. Deng, J. Wang, J. Han, and X. Zhao, Low temperature photoluminescence properties of CsPbBr₃ quantum dots embedded in glasses, *Phys. Chem. Chem. Phys.* **19**, 17349 (2017).
- [19] Y. Ye, W. Zhang, Z. Zhao, J. Wang, C. Liu, Z. Deng, X. Zhao, and J. Han, Highly luminescent cesium lead halide perovskite nanocrystals stabilized in glasses for light emitting applications, *Adv. Opt. Mater.* **7**, 1801663 (2019).
- [20] E. V. Kolobkova, M. S. Kuznetsova, and N. V. Nikonorov, Perovskite CsPbX₃ (X = Cl, Br, I) nanocrystals in fluorophosphate glasses, *J. Non-Cryst. Solids* **563**, 120811 (2021).
- [21] E. Kirstein, D. R. Yakovlev, M. M. Glazov, E. A. Zhukov, D. Kudlacik, I. V. Kalitukha, V. F. Sapega, G. S. Dimitriev, M. A. Semina, M. O. Nestoklon, E. L. Ivchenko, N. E. Kopteva, D. N. Dirin, O. Nazarenko, M. V. Kovalenko, A. Baumann, J. Höcker, V. Dyakonov, and M. Bayer, The Landé factors of electrons and holes in lead halide perovskites: universal dependence on the band gap, *Nat. Commun.* **13**, 3062 (2022).
- [22] See Supplemental Material at <http://link.aps.org/supplemental/10.1103/PhysRevB.109.235301> for models of the NCs energy structure, PL temperature quenching, PL dynamics, and for temperature-dependent spectra of the CsPbBr₃ samples, and which includes Refs. [18,21,23–27].
- [23] L. D. Landau and E. M. Lifshits, *Quantum Mechanics: Non-Relativistic Theory* (Butterworth-Heinemann, Oxford, 1991).
- [24] S. Flügge, *Practical Quantum Mechanics* (Springer, New York, 2012).
- [25] W. Elsasser, Atomare wellenfunktion im impulsraum, *Z. Phys.* **81**, 332 (1933).
- [26] Q. A. Akkerman, G. Rainò, M. V. Kovalenko, and L. Manna, Genesis, challenges and opportunities for colloidal lead halide perovskite nanocrystals, *Nat. Mater.* **17**, 394 (2018).
- [27] S. Savchenko, A. Vokhmintsev, and I. Weinstein, Activation energy distribution in thermal quenching of exciton and defect-related photoluminescence of InP/ZnS quantum dots, *J. Lumin.* **242**, 118550 (2022).
- [28] D. R. Yakovlev, S. A. Crooker, M. A. Semina, J. Rautert, J. Mund, D. N. Dirin, M. V. Kovalenko, and M. Bayer, Exciton-polaritons in CsPbBr₃ crystals revealed by optical reflectivity in high magnetic fields and two photon spectroscopy, *Phys. Status Solidi RRL* **18**, 2300407 (2024).
- [29] K. Zheng, K. Židek, M. Abdellah, M. E. Messing, M. J. Al-Marri, and T. Pullerits, Trap states and their dynamics in organometal Halide perovskite nanoparticles and bulk crystals, *J. Phys. Chem. C* **120**, 3077 (2016).
- [30] H. Yuan, E. Debroye, E. Bladt, G. Lu, M. Keshavarz, K. P. F. Janssen, M. B. J. Roeffaers, S. Bals, E. H. Sargent, and J. Hofkens, Imaging heterogeneously distributed photo-active traps in perovskite single crystals, *Adv. Mater.* **30**, 1705494 (2018).
- [31] N. Droseros, G. Longo, J. C. Brauer, M. Sessolo, H. J. Bolink, and N. Banerji, Origin of the enhanced photoluminescence quantum yield in MAPbBr₃ perovskite with reduced crystal size, *ACS Energy Lett.* **3**, 1458 (2018).
- [32] A. Forde, J. A. Fagan, R. D. Schaller, S. A. Thomas, S. L. Brown, M. B. Kurtz, R. J. Petersen, D. S. Kilin, and E. K. Hobbie, Brightly luminescent CsPbBr₃ nanocrystals through ultracentrifugation, *J. Phys. Chem. Lett.* **11**, 7133 (2020).
- [33] S. Rudin, T. L. Reinecke, and B. Segall, Temperature-dependent exciton linewidths in semiconductors, *Phys. Rev. B* **42**, 11218 (1990).
- [34] M. Bayer and A. Forchel, Temperature dependence of the exciton homogeneous linewidth in In_{0.60}Ga_{0.40}As/GaAs self-assembled quantum dots, *Phys. Rev. B* **65**, 041308(R) (2002).
- [35] D. Valerini, A. Cretí, M. Lomascolo, L. Manna, R. Cingolani, and M. Anni, Temperature dependence of the photoluminescence properties of colloidal CdSe/ZnS core/shell quantum dots embedded in a polystyrene matrix, *Phys. Rev. B* **71**, 235409 (2005).
- [36] E. A. Muljarov and R. Zimmermann, Exciton dephasing in quantum dots due to LO-phonon coupling: An exactly solvable model, *Phys. Rev. Lett.* **98**, 187401 (2007).
- [37] M. A. Pérez-Osorio, R. L. Milot, M. R. Filip, J. B. Patel, L. M. Herz, M. B. Johnston, and F. Giustino, Vibrational properties of the organic inorganic halide perovskite CH₃NH₃PbI₃ from theory and experiment: factor group analysis, first-principles calculations, and low-temperature infrared spectra, *J. Phys. Chem. C* **119**, 25703 (2015).
- [38] A. D. Wright, C. Verdi, R. L. Milot, G. E. Eperon, M. A. Pérez-Osorio, H. J. Snaith, F. Giustino, M. B. Johnston, and L. M. Herz, Electron phonon coupling in hybrid lead halide perovskites, *Nat. Commun.* **7**, 11755 (2016).

- [39] C. M. Iaru, A. Brodu, N. J. J. van Hoof, S. E. T. ter Huurne, J. Buhot, F. Montanarella, S. Buhbut, P. C. M. Christianen, D. Vanmaekelbergh, C. de Mello Donega, J. G. Rivas, P. M. Koenraad, and A. Y. Silov, Fröhlich interaction dominated by a single phonon mode in CsPbBr₃, *Nat. Commun.* **12**, 5844 (2021).
- [40] J. Ramade, L. M. Andriambarijaona, V. Steinmetz, N. Goubet, L. Legrand, T. Barisien, F. Bernardot, C. Testelin, E. Lhuillier, A. Bramati, and M. Chamarro, Fine structure of excitons and electron hole exchange energy in poly-morphic CsPbBr₃ single nanocrystals, *Nanoscale* **10**, 6393 (2018).
- [41] H. Shi, X. Zhang, X. Sun, R. Chen, and X. Zhang, Direct and indirect recombination and thermal kinetics of excitons in colloidal all-inorganic lead halide perovskite nanocrystals, *J. Phys. Chem. C* **123**, 19844 (2019).
- [42] W. Wu, W. Liu, Q. Wang, Q. Han, and Q. Yang, Temperature-dependent photoluminescence of pure and Mn-doped CsPbCl₃ nanocrystals, *J. Alloys Compd.* **787**, 165 (2019).
- [43] A. A. Lohar, A. Shinde, R. Gahlaut, A. Sagdeo, and S. Mahamuni, Enhanced photoluminescence and stimulated emission in CsPbCl₃ nanocrystals at low temperature, *J. Phys. Chem. C* **122**, 25014 (2018).
- [44] T. T. Pham, H. Lee, J. Lee, and W. J. Chung, Perovskite nanocrystal-embedded glasses for photonic applications, *J. Korean Ceram. Soc.* **59**, 749 (2022).
- [45] K. Wei, Z. Xu, R. Chen, X. Zheng, X. Cheng, and T. Jiang, Temperature-dependent excitonic photoluminescence excited by two-photon absorption in perovskite CsPbBr₃ quantum dots, *Opt. Lett.* **41**, 3821 (2016).
- [46] C. Wolf and T.-W. Lee, Exciton and lattice dynamics in low-temperature processable CsPbBr₃ thin-films, *Mater. Today Energy* **7**, 199 (2018).
- [47] V. N. Abakumov, V. I. Perel, and I. N. Yassievich, *Nonradiative Recombination in Semiconductors in "Modern Problems in Condensed Matter Science," Vol. 33* (Elsevier, Amsterdam, 1991).
- [48] G. E. Cragg and A. L. Efros, Suppression of Auger processes in confined structures, *Nano Lett.* **10**, 313 (2010).
- [49] C. Javaux, B. Mahler, B. Dubertret, A. Shabaev, A. V. Rodina, A. L. Efros, D. R. Yakovlev, F. Liu, M. Bayer, G. Camps, L. Biadala, S. Buil, X. Quelin, and J.-P. Hermier, Thermal activation of non-radiative Auger recombination in charged colloidal nanocrystals, *Nat. Nanotechnol.* **8**, 206 (2013).
- [50] D. Rossi, T. Qiao, X. Liu, M. Khurana, A. V. Akimov, J. Cheon, and D. H. Son, Size-dependent dark exciton properties in cesium lead halide perovskite quantum dots, *J. Chem. Phys.* **153**, 184703 (2020).
- [51] E. V. Shornikova, L. Biadala, D. R. Yakovlev, V. F. Sapega, Y. G. Kusrayev, A. A. Mitioglu, M. V. Ballottin, P. C. M. Christianen, V. V. Belykh, M. V. Kochiev, N. N. Sibeldin, A. A. Golovatenko, A. V. Rodina, N. A. Gippius, A. Kuntzmann, Y. Jiang, M. Nasilowski, B. Dubertret, and M. Bayer, Addressing the exciton fine structure in colloidal nanocrystals: The case of CdSe nanoplatelets, *Nanoscale* **10**, 646 (2018).
- [52] V. V. Belykh, M. L. Skorikov, E. V. Kulebyakina, E. V. Kolobkova, M. S. Kuznetsova, M. M. Glazov, and D. R. Yakovlev, Submillisecond spin relaxation in CsPb(Cl,Br)₃ perovskite nanocrystals in a glass matrix, *Nano Lett.* **22**, 4583 (2022).
- [53] J. Feldmann, G. Peter, E. O. Göbel, P. Dawson, K. Moore, C. Foxon, and R. J. Elliott, Linewidth dependence of radiative exciton lifetimes in quantum wells, *Phys. Rev. Lett.* **59**, 2337 (1987).
- [54] V. V. Belykh and M. V. Kochiev, Heating by exciton and biexciton recombination in GaAs/AlGaAs quantum wells, *Phys. Rev. B* **92**, 045307 (2015).